International Journal of Physics and Applications

E-ISSN: 2664-7583
P-ISSN: 2664-7575
IJOS 2025; 7(2): 44-51

www.physicsjournal.in
Received: 27-05-2025
Accepted: 25-06-2025

Megha Agari
Department of Physics, Govt. Degree College, Shitlakhet-Almora, Uttarakhand, India

Lalan Prasad
Department of Physics, Govt. Degree College, Shitlakhet-Almora, Uttarakhand, India

Corresponding Author:
Megha Agari
Department of Physics, Govt. Degree College, Shitlakhet-Almora, Uttarakhand, India

Magnetic phenomena which is similar to atmospheric phenomena: Result from the Northern lights or aurora features with solar wind, interplanetary magnetic field, and geomagnetic activity

Megha Agari and Lalan Prasad

DOI: https://doi.org/10.33545/26647575.2025.v7.i2a.169

Abstract
Auroral emissions occur as a result of the influx of high-energy electrons, as well as protons, which descend along the magnetic field lines, thereby infiltrating the Earth's atmospheric layers. Luminous and extensive auroras observed in the polar zones indicate perturbations within the magnetosphere and solar wind; such perturbations, in numerous cases, have the potential to forecast auroral phenomena. The depiction of the auroral oval serves as a critical indicator of space weather phenomena. A comprehensive 27-year investigation (spanning from 1 January 1997 to 20 July 2024) was undertaken focusing on various magnetic field and solar wind parameters—specifically, the interplanetary magnetic field, solar wind proton density, solar wind plasma flow velocity, flow pressure, among others—utilizing the KP index as a framework for analysis. The superposed epoch methodology is employed to analyze events classified as active and minor (G1), moderate (G2), strong (G3), severe (G4), and extreme (G5) storms, with Spearman's rank correlation employed to demonstrate a monotonic relationship across all parameters investigated. The correlation observed between the rankings of the interplanetary magnetic field and the KP index registers at +0.9 during G2 and G3 storm events. Furthermore, the solar wind plasma velocity and flow pressure exhibit correlations of +0.8 and +0.7, respectively, concerning active and G1 storm classifications. This manuscript examines the intricacies of the Interplanetary Magnetic Field (IMF) in conjunction with the characteristics of solar wind, particularly regarding auroral phenomena and the interaction between solar wind and both the Earth and its magnetosphere.

Keywords: Solar wind, geomagnetic field, magnetosphere, magnetic reconnection, aurora

1. Introduction
The seminal scientific dissertation regarding the aurora borealis was disseminated by Marcello Squarcialupi; his treatise, De Coeloardore, meticulously documented the aurora phenomenon observed on 10 September 1580, providing a comprehensive analysis of relevant data, morphology, chromatic attributes, orientation, and variability (Kazmer *et al*., 2016) [26]. High-energy particles from the solar wind (SW) are introduced into the Earth's Polar Regions —both northern and southern—before the geomagnetic field (GMF) lines, subsequently colliding with atoms and molecules in the upper atmosphere to induce the auroral display. These auroras predominantly manifest within latitudinal bands ranging from approximately 60º to 75º in both the northern and southern hemispheres, centered around the Earth's magnetic poles, a phenomenon referred to as the "auroral oval" (Akasofu, 1964; Feldstein, 1963; Rostoker *et al*., 1980; Baker *et al*., 1996) [1, 14, 43, 3]. The intensity, along with the geographical positioning of the aurora ovals, reflects the distribution of particle precipitation, which represents critical physical parameters within the space environment and magnetospheric dynamics, thereby influencing the magnetosphere, ionosphere, and thermosphere (Hu *et al*., 2021) [22]. Research has demonstrated that the intensity of the aurora oval can be affected by a multitude of space weather factors. For instance, the relationship between the interplanetary magnetic field (IMF) and the solar wind exhibits a stronger association with the dayside aurora, while a comparatively weaker correlation is observed with the nightside aurora (Hu *et al*., 2012; Liou *et al*., 1998) [23, 28]. The aurora borealis, commonly referred to as the northern lights, can be observed in countries such as Norway, Finland, Alaska, Russia, Iceland, and Greenland, among others. Conversely, the aurora Australis, or southern lights, is predominantly witnessed in Antarctica, with infrequent sightings in Australia. Furthermore, an anomalous occurrence in

April 2023 was recorded, wherein low-latitude auroras were captured by an all-sky camera located at Hanle, Ladakh, India (33º N geographic latitude (GGLat)) (Vichare *et al*., 2024) [50]. An increase in the convective electric field generates significant currents within the ionosphere, resulting in the auroral electrojet, which is detected through magnetic field measurements (McPherron 1972; Newell and Gjerloev 2011; Behera *et al*., 2015) [34, 36, 4]. Notable optical emissions in the sub-auroral region include Isolated Proton Aurora (IPA), Stable Aurora Red (SAR), and Strong Thermal Emission Velocity Enhancement (STEVE) (Gallardo-Lacourt *et al*., 2021; Nishimura *et al*., 2022) [16, 38]. STEVE is found in the sub-auroral region, south of the aurora oval, characterized by its narrow latitude but broad longitude (Gallardo-Lacourt, Nishimura, *et al*., 2018) [17]. The interaction between the solar wind and the Earth creates a natural laboratory for examining how stars interact with magnetized planets. During this interaction, magnetic flux is transferred from the dayside to the nightside through magnetic reconnection, provided the interplanetary magnetic field (IMF) connects with the geomagnetic field (GMF) at the dayside magnetopause. As the IMF moves away from the sun, it draws the newly formed flux tube (IMF+GMF) towards the nightside (Fasel *et al*., 2024) [13]. Magnetic reconnection happens along two magnetic neutral lines: first at the subsolar magnetopause and secondly within the geomagnetic tail (Dungey *et al*., 1961) [11]. This process is thought to be the main mechanism for transferring solar wind momentum, along with energy, into the magnetosphere. To study magnetic reconnection at the dayside magnetopause, high-latitude satellite observations were utilized for the first time (Haerendel *et al*., 1978; Russell and Elphic, 1979) [21, 44].

Thomsen (2004) [49] found that the KP index serves as an adequate measure of magnetospheric convection, as the degree of magnetic disturbance observed at sub-auroral stations is dependent on their proximity to the auroral zone, while strong currents in the auroral region correlate with the plasma sheet. The convection electric field has a significant impact on the inner boundary of the plasma sheet, making sub-auroral stations particularly sensitive to convection (Thomsen, 2004) [49]. The KP index is widely used in the assessment of ionospheric and magnetospheric research due to its extensive historical record and its relationship with magnetospheric convection (Thomsen, 2004) [49].

(Nakai *et al*., 1983) [35] And (Boudouridis *et al*., 2003) [5] analyzed the behavior of the auroral oval in response to the interplanetary magnetic field (IMF) and solar wind dynamic pressure. Specifically, Nakai *et al*. (1983) [35 examined the equatorward boundaries during periods when the IMF shifts southward, noting that these boundaries tend to be at lower latitudes in comparison to times of northward IMF. The IMF serves as the key driver of magnetic reconnection and activity within the magnetosphere due to the solar wind. Its notable influence has been documented over several years (e.g., Akasofu, 1980; Boyle *et al*., 1997; Cowley, 1984; Rich and Hairston, 1994) [2, 6, 9, 40]. Although additional components of the IMF affect auroral brightness, their effects are not as pronounced as those of B_Z. In the northern hemisphere, auroral intensity in the pre-midnight sector is greater during negative B_Y conditions than during positive B_Y (Liou *et al*., 1998) [28]. The authors attributed this B_Y asymmetry to the partial penetration of IMF B_Y by solar wind into the magnetosphere (Fairfield, 1979; Cowley and Hughes, 1983; Lui, 1984; Wing *et al*., 1955) [12, 10, 31, 51], which leads to an interhemispheric current that may either contribute to or subtract from existing field-aligned currents. A dawn-dusk asymmetry related to various high-latitude magnetospheric and ionospheric phenomena, including the aurora, can be linked to the east-west (y) component of the IMF (Liou *et al*., 2019) [30]. Discussing the north-south (z) component, Shue *et al*. (2002) [46] found that aurora brightness is more strongly dependent on the IMF-B_Z effect than on solar wind density and velocity. When the IMF is directed northward, the electric field from the solar wind introduced into the polar cap is diminished. Nonetheless, the viscous mechanism can create a small area of polar cap potential on the flank (Reiff *et al*., 1981) [42], leading to a slight convection flow due to minimal field-aligned currents along with weak auroral brightness. Conversely, when the IMF is directed southward, the solar wind creates a robust polar cap potential that induces powerful convection flows, heightened auroral brightness, and intensified field-aligned currents. Shue *et al*. (2001a) [47] indicated that the increase in auroral brightness observed in the early morning sector is a result of higher background conductance. The intensity of the aurora tends to be greater in this sector during the summer compared to the winter. Numerous studies have indicated that sudden increases in solar wind dynamic pressure have a significant effect on the magnetosphere-ionosphere system of the Earth (e.g., Boudouridis *et al*., 2003; Liou, 2006) [5, 29]

The full comprehension of the physical mechanisms that give rise to various types of auroras remains elusive, but the fundamental principle suggests an interaction between solar wind and the Earth's magnetosphere (Gupta *et al*., 2020) [20]. This research highlights the characteristics observed during the northern lights and fluctuations in parameters such as the interplanetary magnetic field (IMF), B_Y component, solar wind proton density, solar wind plasma flow speed, flow pressure, and the KP index.

2. Data and Methods of Analysis

The KP index reflects geomagnetic activity on a global scale, as observed through 13 magnetic observatories located at midlatitudes (Mayaud, 1980) [33]. The KP index is widely used to represent geomagnetic activity and has demonstrated its value in a long historical archive dating back to the 1930s (Carbary *et al*., 2005) [7]. The scaled KP indices utilized in this analysis are sourced from the OMNI site of NASA (https://omniweb.gsfc.nasa.gov/form/dx1.html), with KP values expressed as multiples of 10, represented as KP*10. For instance, a KP value of 6 indicates 60 (KP*10), which is helpful for certain datasets, particularly in the analysis of solar wind influences on geomagnetic storms, as noted by Richardson *et al*. (2012) [41].

According to NOAA's classification of storm sizes (http://www.swpc.noaa.gov/NOAAscales/), KP values of 4 and 5 signify active and minor (G1) storms, respectively, while KP values of 6 and 7 signify moderate (G2) and strong (G3) storms. KP values of 8 and 9 indicate severe (G4) and extreme (G5) storms, respectively. G4 and G5 storms are classified as "major" storms based on the criteria set by Gosling *et al*. (1991) [19]; G1 represents a small storm, G2 a medium storm, and G3 a relatively large storm. Primarily, KP*10 indices are gathered using Swarm VRE, with data compiled at the midpoint of KP*10 values of 30, 35, 40, 45, 50, 55, 60, 70, 80, and 90. The occurrences of KP*10 values exceeding 60 are significantly lower when compared to those below 60, which leads to a width of 10 instead of 5 (Shi *et al*., 2022). For the initial 27 years of data with a 1-day time resolution from January 1, 1997, to July 20, 2024, superposed epoch analysis was conducted by examining ±36 values around the specific event. We derive conclusions based on

Spearman's rank correlation coefficients, as the correlation coefficient ranges from -1 to +1. When the curve approaches ±1, it indicates a strong correlation; conversely, when it nears zero, it signifies a weak correlation (Katz, 1988; Karki *et al*., 2020) [25, 24].

3. Feature of the KP index with the magnetic field and solar wind parameters

The spatial distribution and morphology of the auroral oval are influenced by geomagnetic activity, which is quantitatively assessed through the KP index. This index is derived from K indices recorded by 13 sub-auroral observatories, wherein K is determined by two horizontal components of geomagnetic data, serving as a geomagnetic index specific to each observatory. The intensity of the KP index may enhance the understanding of the position and luminosity of the auroral oval (Feng *et al*., 2025) [15]. In contemporary research, the application of machine learning methodologies to predict the KP index has gained considerable traction, thereby motivating our investigation into auroral characteristics that are contingent upon the KP index. Novel applications about the KP index continue to be developed. Choi *et al*. (2011) [8] explored anomalies impacting commercial satellites situated in geostationary orbits, revealing a notable correlation between the KP index and the frequency of these anomalies. As per O'Brien (2009) [39], the likelihood of surface charging in geosynchronous satellites peaks when the KP index ranges from 4 to 7. This research provides a correlational analysis of the KP index in conjunction with various interplanetary magnetic field (IMF) and solar wind parameters for KP index values extending from 4 to 9. An aurora signifies the interplay between the magnetospheric and ionospheric systems. The frequency of auroral arcs increases during periods of a southward interplanetary magnetic field (IMF), whereas it decreases during a northward IMF (Lassen *et al*., 1978) [27].

3.1 Active and G1 storms features with solar wind and magnetic field parameters

The solar wind plasma velocity and the KP index demonstrate a significant cross-correlation coefficient of 0.48; in contrast, the interplanetary magnetic field (IMF) component B_Z exhibits a diminished cross-correlation coefficient of less than 0.26 (Gholipour *et al*., 2004) [18]. Within the scope of this investigation, at the zero-day mark, the B_Z component is characterized by an exceedingly low magnitude of approximately 1.6 nT, associated with auroras occurring during both active and minor geomagnetic storms. A variance in the IMF B_Z exhibiting a greater magnitude has been observed at a low KP index for ±36 days. The maximum peak inclination was ascertained to occur between 10 and 20 days before the event (top panel of Figure 1). Nevertheless, in contrast to these assertions, Newell *et al*. (2008) [37] elucidated a multifaceted relationship in which solar wind velocity, Bt (the magnitude of IMF-B_Y and IMF-B_Z), density, and clock angle (derived from IMF-B_Y and IMF-B_Z) yielded a cross-correlation coefficient of 0.86 concerning the KP index. The magnitude of the interplanetary magnetic field (IMF) fluctuates to a maximum of 9.5 nT for elevated KP at the zero-day interval, subsequently decreasing and oscillating between 6 nT and 7.5 nT for a low KP index over 5-36 days (bottom panel of Figure 1). The fluctuation of IMF B_Y for both -36 and +36 days is approximately observed at a lower KP index, taking into account its magnitude; however, at the zero-day mark, its magnitude is recorded in the middle of 0.4 nT and 0.6 nT for a higher KP index (middle panel of Figure 1).

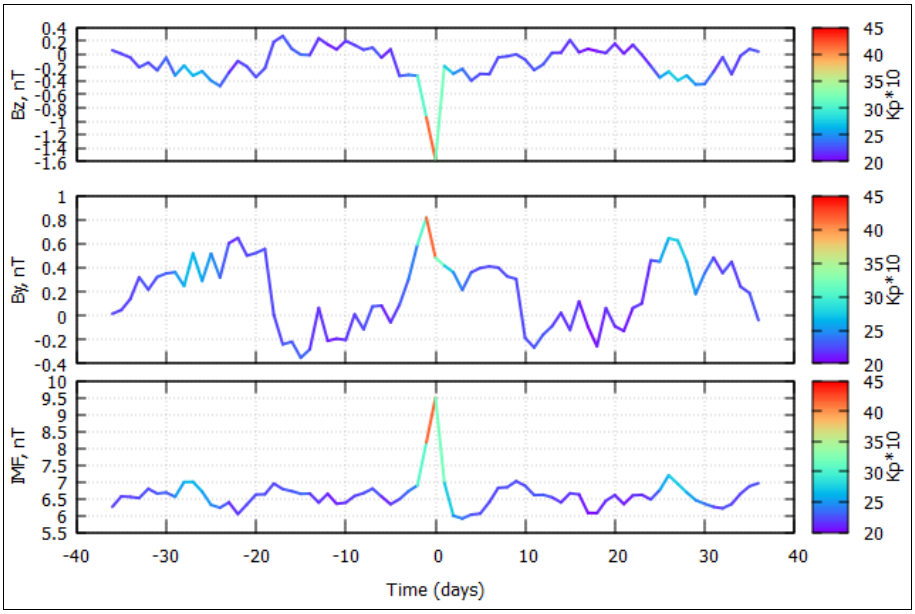

Fig 1: A superposed epoch analysis encompassing 27 years of empirical data about active and G1 storms (for KP values of 3 and 4) is presented; the lower, middle, and upper panels depict the fluctuations of the interplanetary magnetic field (IMF), B_Y, and B_Z in correspondence with the KP index, respectively.

An earlier investigation (Snyder *et al*., 1963) [48] indicated a robust correlation between the KP index and the velocity of solar wind plasma. In the present study, our analysis reveals that the ranked values of solar wind plasma velocity exhibit a strong monotonic association (+0.8) with the ranked values of the KP index (refer to Table 1). This type of correlation is appropriate as the interaction significantly influences the magnetospheric convection electric field, which becomes evident as the solar wind rapidly moves through Earth (Thomsen, 2004) [49]. In the temporal analysis extending 36 days before and after the event, the solar wind plasma velocity predominantly remains below approximately 500 km/s at a low KP index. However, in the three days preceding the event, the solar wind plasma velocity increases concomitantly with the KP index, peaking at approximately 540 km/s on the day of the event for both active and G1

storms. The most significant peak is observed between 0- and 5-days post-event (illustrated in the bottom panel of Figure 2). The flow pressure fluctuates between 3.2 and 3.8 nPa for active and minor auroras; after the event, the flow pressure experiences a continuous decline, stabilizing between 2 and 2.8 nPa throughout +1 to +36 days (as depicted in the middle panel of Figure 2). The proton density of the solar wind reaches a peak value of 8 N/cm³ before the event, decreasing to 7.5 N/cm³ on the day of the event. The likelihood for the occurrence of active and minor auroras is maximized between these two density values (as shown in the top panel of Figure 2).

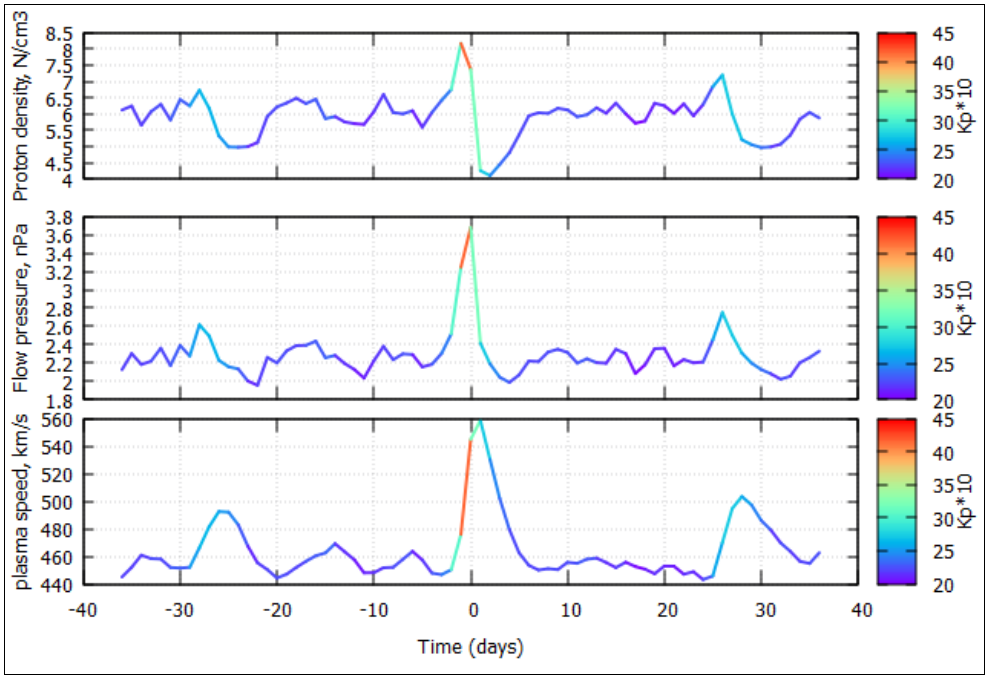

Fig 2: Temporal study of solar wind proton density, flow pressure, and solar wind plasma speed encompassing 27 years of empirical data for active and G1 storms is presented; the upper, middle, and lower panels delineate the variations of diverse parameters concerning the KP index.

3.2 Feature of G2 and G3 storms with solar wind and magnetic field parameters

Upon examination of the luminous auroras present in the Earth's atmosphere, it is noted that the interplanetary magnetic field (IMF) exhibits a significant correlation of approximately +0.9 with the KP index. At the initial observation point, the magnitude of the IMF reaches 16 nT for elevated KP values, whereas, in the preceding and subsequent 36-day intervals, the magnitude of the IMF remains below 10 nT (refer to the lower panel of Figure 3). In analyzing the north-south component BZ, it is observed to have a feeble correlation of -0.4, with the lowest magnitude (negative) occurring at the zero-day mark; conversely, across ±36 days, this component fluctuates between -1.5 and +2 nT (as illustrated in the upper panel of Figure 3).

Conversely, the east-west component of the Interplanetary Magnetic Field (B_Y) exhibits a moderate correlation coefficient of +0.5 with the KP index. At the zero-day threshold, the maximum inclination has been observed, wherein the magnitude of B_Y attains a value of 3 nT during episodes of intense auroras (as illustrated in the central panel of Figure 3).

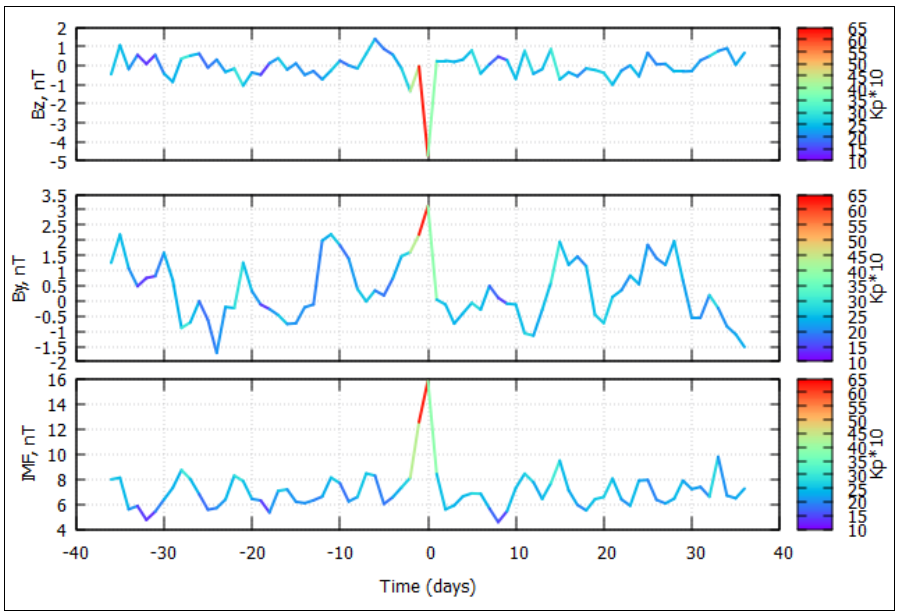

Fig 3: In the KP index, alterations in the interplanetary magnetic field (IMF), along with its east-west (B_Y) and north-south (B_Z) components, are discernible when bright auroras, or northern lights, manifest near the Earth's atmosphere as a result of G2 and G3 storms.

During the G2 and G3 geomagnetic storms, the mean proton density of the solar wind is quantified at 6.1 N/cm3. The Spearman rank correlation coefficient computed between the proton density of the solar wind and the KP index reveals a moderate positive correlation of +0.7, thereby indicating a robust positive association within the framework of auroral phenomena. The peak declination was observed within the temporal window of (0-5) days preceding the event, at which point the zero-day magnitude of solar wind proton density is recorded at 7 N/cm3, whereas the minimal inclination is noted between (0-5) days after the event (refer to the top panel of Figure 4).

The ranked datasets about solar wind plasma velocity and flow pressure exhibit commendable correlations of +0.8 and +0.9, respectively. The apex of the fluctuations in solar wind plasma velocity is identified on the zero day, with an average speed calculated at 650 km/s (as illustrated in the bottom panel of Figure 4). The flow pressure predominantly oscillates between 1.5 nPa and 3.5 nPa for the temporal intervals of (5-36) days before and after the event, with the maximum inclination recorded within (0-5) days before the event, during which the flow pressure escalates to 6 nPa in correlation with auroral activity (as depicted in the middle panel of Figure 4).

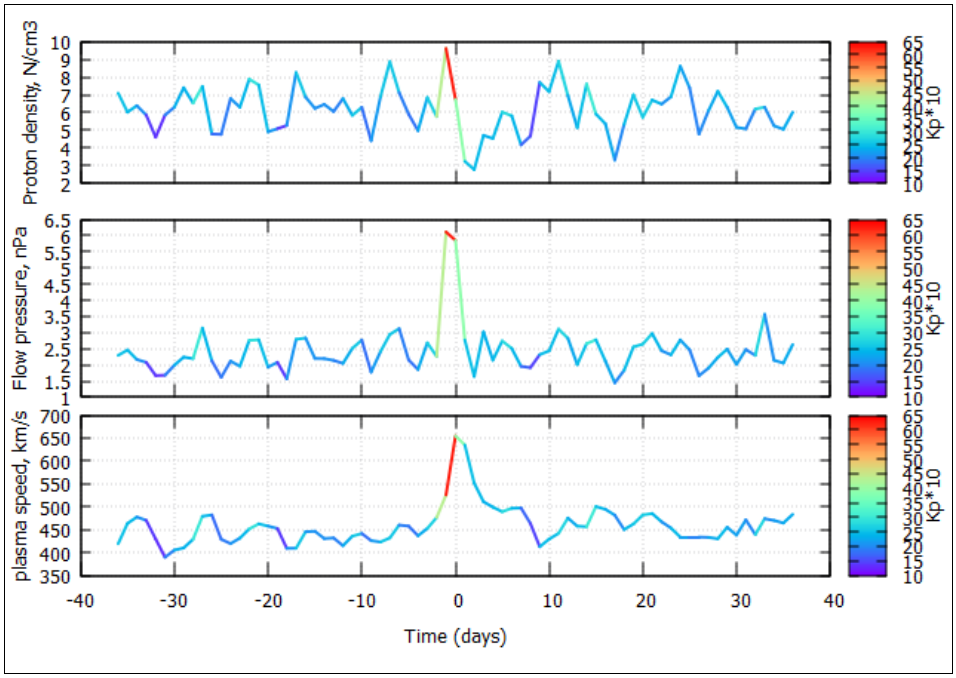

Fig 4: For luminous auroras (KP=6, 7), the variations in the solar wind plasma speed, the solar wind proton density, and the flow pressure are assessed over a time frame of -36 and +36 days.

Table 1: Spearman's rank correlation coefficients for solar wind, IMF, and KP variables.

(Active and Minor storm)		(Moderate and strong storms)	
IMF, nT	0.7	IMF, nT	0.9
B_Y (GSM), nT	0.6	B_Y (GSM), nT	0.5
B_Z, (GSM), nT	-0.1	B_Z (GSM), nT	-0.4
Solar wind plasma speed, km/s	0.8	Solar wind plasma speed, km/s	0.8
Solar wind proton density, N/cm^3	0.4	Solar wind proton density, N/cm^3	0.7
Flow pressure, nPa	0.7	Flow pressure, nPa	0.9
Plasma flow longitude, deg	0.5	Plasma flow longitude, deg	0.7
Plasma flow latitude, deg	0.2	Plasma flow latitude, deg	0.5

4. Conclusion

In this research, we discuss how the KP index varies with various parameters, including solar wind plasma speed (km/s), flow pressure (nPa), solar wind proton density (N/cm³), interplanetary magnetic field (IMF), and its east-west component (IMF-B_Y), as well as the north-south component (IMF-B_Z). These factors are crucial for predicting magnetic events analogous to atmospheric phenomena. Through a correlational analysis, we draw the following conclusions.

1. A robust correlation coefficient of +0.7 exists between the interplanetary magnetic field (IMF) and the KP index for active and G1 storms; this correlation increases to +0.9 for G2 and G3 storms, thereby signifying a pronounced monotonic relationship between these two variables, which proves to be more efficacious to magnetospheric activity and magnetic reconnection phenomena. The east-west component, denoted as IMF B_Y, exhibits a correlation of +0.6 for active and G1 storms, and +0.5 for G2 and G3 storms, thereby indicating a moderate influence on auroral activity that facilitates an asymmetrical north-south distribution within the geomagnetic field of the Earth.
2. As previously stated, the brightness of auroras is less influenced by the solar wind proton density than by the effects of IMF-B_Z. In this analysis, for active and G1 storms, the brightness of the auroras shows only a weak dependence on IMF-B_Z this result can be elucidated through the peak identified at the zero-day mark in the aforementioned illustration (upper section of Figure 1), reflected in a low Spearman's rank correlation of -0.1, while the correlation with solar wind proton density is

also weak, at +0.4 concerning the KP index. Conversely, during G2 and G3 storm phases, the relationship with IMF B_Z is weaker at -0.4 when compared to the solar wind proton density, which shows a stronger correlation of +0.7. Nevertheless, this weak correlation does not have a significant impact on the control of density.

3. The velocity of solar wind plasma exhibits a pronounced monotonic correlation with the KP index as evidenced in this study; during periods of active and G1 storms, solar wind traverses the Earth's atmosphere at an elevated velocity, averaging 464 km/s, with peak measurements reaching 560 km/s within the temporal window of +1 to +5 days. In contrast, the mean velocity recorded during G2 and G3 storms is 459 km/s, and at the zero-day mark, it surpasses 650 km/s. The influence of solar wind plasma velocity on auroral luminosity is notably substantial, demonstrating a contribution coefficient of +0.8, This association exerts a significant effect on the electric field related to magnetospheric convection during active intervals and G1, G2, and G3 storm events.
4. The solar wind flow pressure is notably strong during active, G1, G2, and G3 storm phases. The typical pressure observed during active and G1 storms is around 3.6 nPa, exhibiting a strong monotonic correlation of +0.7 with KP. In contrast, the maximum pressure recorded during G2 and G3 storms is about 5.5 nPa at zero-day, and a high Spearman's rank correlation of +0.9 has been found. This often coincides with the appearance of a bright aurora. The longitudinal fluctuation of plasma flow during periods of active and G1 storms is notably substantial, exhibiting a correlation coefficient of +0.5 with the KP index and a maximum inclination observed at zero days, whereas the latitudinal fluctuation demonstrates a correlation of +0.2. Before the 20 to 30-day mark, the maximum inclination is attained, with the minimum inclination occurring between +10 and +20 days (Figure 5). Furthermore, in the context of G2 and G3 storms, the longitudinal and latitudinal fluctuations of plasma flow are characterized as moderate, with values recorded at +0.7 and +0.5, respectively. The apex of plasma flow concerning longitude is noted to occur between 20 and 30 days before the event, while the nadir of plasma flow is identified at 10 days after the event. Conversely, in the variation of plasma flow with latitude, the highest peak is found between 20 to 30 days after the event, where the lowest peak is found at 10 days before the event. Illustration of plasma flow with longitude and latitude during the bright aurora present in Figure 6. In contrast, the fluctuation of plasma flow with latitude exhibits its apex approximately 20 to 30 days after the occurrence of the event, while the decline is observed 10 days before the event. A depiction of plasma flow in correlation with both longitude and latitude amidst the luminous aurora is illustrated in Figure 6.

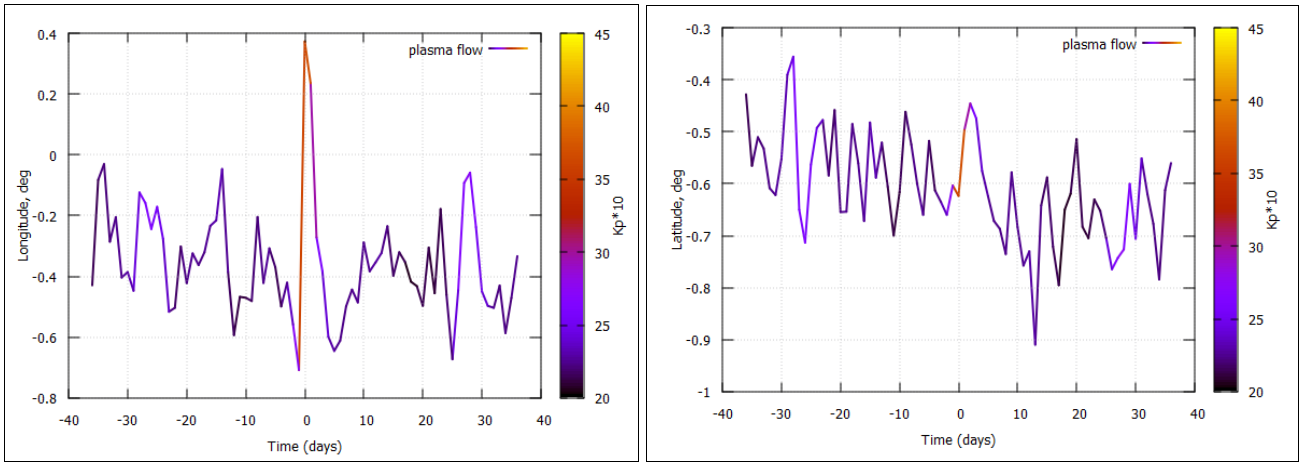

Fig 5: A superposed epoch diagram illustrating 27 years of data, specifically regarding auroras concerning active and G1 geomagnetic storms; a delineation of plasma flow fluctuations with KP at longitudinal (left) and latitudinal (right) coordinates.

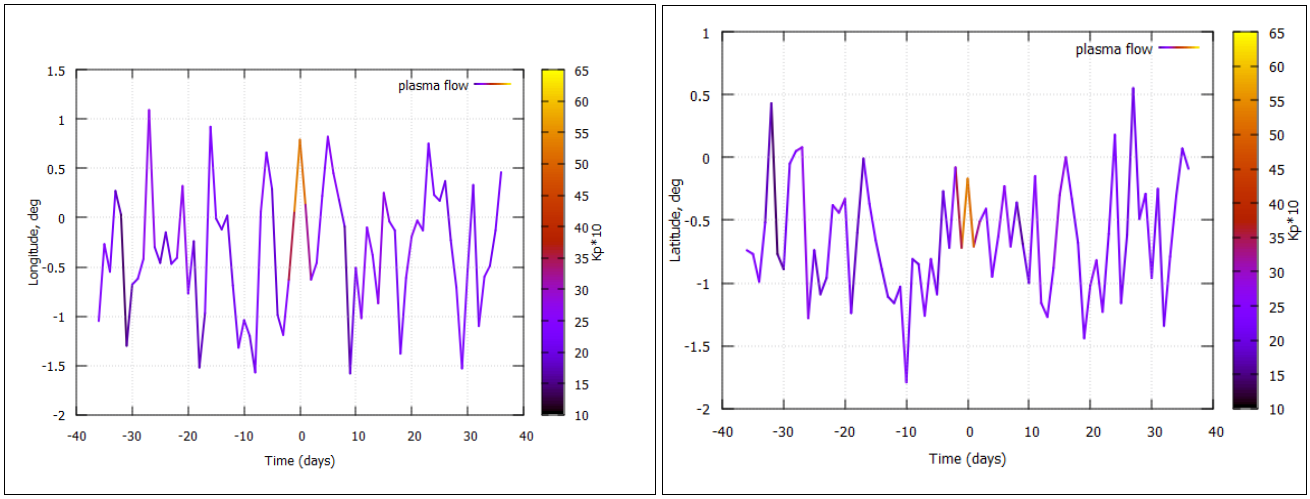

Figure 6. When auroras, commonly referred to as northern lights, manifest with notable brightness in proximity to the Earth's atmosphere as a result of moderate to strong geomagnetic storms, a delineation of plasma flow fluctuations with KP at longitudinal (left) and latitudinal (right) coordinates is observed.

Ethical declaration
not applicable

Acknowledgment
The authors appreciate the Journal of Solar Physics for providing the Content Page Service for each new issue, which helps us stay updated. The reliable data utilized in our experiments was sourced from NASA and NOAA websites, as well as from data obtained through missions like the Advanced Composition Explorer (ACE) spacecraft, Ulysses, and DSCOVR. We also extend our thanks to the administration of the Government. Degree College, Shitlakhet-263678, Uttarakhand, for offering us the necessary workstation. Funding is not applicable for this research.

5. References

1. Akasofu SI. The latitudinal shift of the auroral belt. J Atmos Terr Phys. 1964;26(12):1167-1174. https://doi.org/10.1016/0021-9169(64)90125-4
2. Akasofu SI. The solar wind, magnetosphere energy coupling, and magnetospheric disturbances. Planet Space Sci. 1980;28:495-509. https://doi.org/10.1016/0032-0633(80)90031-8
3. Baker DN, Pulkkinen T, Angelopoulos V, Baumjohann W, McPherron R. Neutral line model of substorms: Past results and present view. J Geophys Res Space Phys. 1996;101:12975-13010. https://doi.org/10.1029/95JA03753
4. Behera JK, Sinha AK, Singh AK, Vichare G, Dhar A, Labde S, Jeeva K. Substorm-related CNA near equatorward boundary of the auroral oval about interplanetary conditions. Adv Space Res. 2015;56:28-40. http://dx.doi.org/10.1016/j.asr.2015.03.036
5. Boudouridis A, Zesta E, Lyons LR, Anderson PC, Lummerzheim D. Effect of solar wind pressure pulses on the size and strength of the auroral oval. J Geophys Res. 2003;108(A4):8012. https://doi.org/10.1029/2002JA009373
6. Boyle CB, Reiff PH, Hairston MR. Empirical polar cap potentials. J Geophys Res. 1997;102(A1):111-125. https://doi.org/10.1029/96JA01742
7. Carbary JF. A KP-based model of auroral boundaries. Space Weather. 2005;3:S10001. https://doi.org/10.1029/2005SW000162
8. Choi HS, *et al*. Analysis of GEO spacecraft anomalies: Space weather relationships. Space Weather. 2011;9:06001. https://doi.org/10.1029/2010SW000597
9. Cowley SWH. Solar wind control of magnetospheric convection. In: Battrick B, Rolfe E, editors. Achievements of the International Magnetospheric Study (IMS). Netherlands: European Space Agency; 1984. p. 483-494.
10. Cowley SWH, Hughes WJ. Observation of an IMF sector effect in the Y-magnetic field component at geostationary orbit. Planet Space Sci. 1983;31:73-90. https://doi.org/10.1016/0032-0633(83)90032-6
11. Dungey JW. Interplanetary magnetic field and the auroral zones. Phys Rev Lett. 1961;6(2):47-48. https://doi.org/10.1103/PhysRevLett.6.47
12. Fairfield DH. Average configuration of the geomagnetic tail. J Geophys Res. 1979;84:1950-1958. https://doi.org/10.1029/JA084iA05p01950
13. Fasel GJ, Lee LC, Lake E, Csonge D, Yonano B, Bradley O, *et al*. Correlation between the solar wind speed and the passage of poleward-moving auroral forms into the polar cap. Front Astron Space Sci. 2024;10:1233060. https://doi.org/10.3389/fspas.2023.1233060
14. Feldstein YI. Some problems concerning the morphology of auroras and magnetic disturbances at high latitudes. Geomagn Aeron. 1963;3:183-192. https://www.osti.gov/biblio/4077408
15. Feng H, Wang D, Shprits YY, Smirnov A, Guo D, Miyoshi Y, *et al*. A KP-driven machine learning model predicting the ultraviolet emission auroral oval. J Geophys Res Mach Learn Comput. 2025;2:e2024JH000543. https://doi.org/10.1029/2024JH000543
16. Gallardo-Lacourt B, Frey H, Martinis C. Proton aurora and optical emissions in the subauroral region. Space Sci Rev. 2021;217(10):10. https://doi.org/10.1007/s11214-020-00776-6
17. Gallardo-Lacourt B, Nishimura Y, Donovan E, Gillies DM, Perry GW, Archer WE, *et al*. A statistical analysis of STEVE. J Geophys Res Space Phys. 2018;123(11):9893-9905. https://doi.org/10.1029/2018ja025368
18. Gholipour A, Lucas C, Araabi BN. Black box modeling of magnetospheric dynamics to forecast geomagnetic activity. Space Weather. 2004;2:S07001. https://doi.org/10.1029/2003SW000039
19. Gosling JT, McComas DJ, Phillips JL, Bame SJ. Geomagnetic activity associated with Earth passage of interplanetary shock disturbances and coronal mass ejections. J Geophys Res. 1991;96:7831-7839. https://doi.org/10.1029/91JA00316
20. Gupta SRN. Review of aurora borealis: Spectacular manifestations of solar wind and atmosphere. Int Res J Sci Eng. 2020;8(1):5-23. http://www.irjse.in
21. Haerendel G, Paschmann G, Sckopke N, Rosenbauer H, Hedgecock PC. The frontside boundary layer of the magnetosphere and the problem of reconnection. J Geophys Res Space Phys. 1978;83(A7):3195-3216. https://doi.org/10.1029/JA083iA07p03195
22. Hu ZJ, Han B, Zhang Y, Lian H, Wang P, Li G, *et al*. Modeling of ultraviolet aurora intensity associated with interplanetary and geomagnetic parameters based on neural networks. Space Weather. 2021;19:e2021SW002751. https://doi.org/10.1029/2021SW002751
23. Hu ZJ, Yang HG, Han DS, Huang DH, Zhang BC, Hu HQ, Liu RY. Dayside auroral emissions controlled by IMF: A survey for dayside auroral excitation at 557.7 and 630.0 nm in Ny-Ålesund, Svalbard. J Geophys Res Space Phys. 2012;117(A2):A02201. https://doi.org/10.1029/2011JA017188
24. Karki M, Silwal A, Chapagain NP, Poudel P, Gautum SP, Mishra RK, Orue YOM. GPS observations of ionospheric TEC variations during the 2015 Mw 7.8 Nepal earthquake. Earth Space Sci Open Arch ESSOAr. 2020. https://doi.org/10.1002/essoar.10504866.1
25. Katz RW. Use of cross-correlation in the search for teleconnections. J R Meteorol Soc. 1988;8:241-253. https://doi.org/10.1002/joc.3370080303
26. Kazmer M, Timar G. The first scientific description of aurora borealis: The 10 September 1580 event in Transylvania, recorded by Marcello Squarcialupi. Geosci Lett. 2016;3:15. https://doi.org/10.1186/s40562-016-0047-2

27. Lassen K, Danielsen C. Quiet time pattern of auroral arcs for different directions of the interplanetary magnetic field in the Y-Z plane. J Geophys Res. 1978;83:5277-5282. https://doi.org/10.1029/JA083iA11p05277
28. Liou K, Newell PT, Meng CI, Brittnacher M, Parks G. Characteristics of the solar wind controlled auroral emissions. J Geophys Res. 1998;103:17543-17557. https://doi.org/10.1029/98JA01388
29. Liou K. Global auroral response to interplanetary media with emphasis on the solar wind dynamic pressure enhancements. In: Tsurutani B, *et al*, editors. Recurrent Magnetic Storms: Corotating Solar Wind Streams. Geophys Monogr Ser. Vol. 167. Washington, D.C: AGU; 2006. p. 197-212. https://doi.org/10.1029/167gm17
30. Liou K, Mitchell E. Effects of the interplanetary magnetic field Y components on the dayside aurora. Geosci Lett. 2019;6:11. https://doi.org/10.1186/s40562-019-0141-3
31. Lui ATY. Characteristics of the cross-tail current in the Earth's magnetotail. In: Potemra TA, editor. Magnetospheric currents. Geophys Monogr Ser. Vol. 28. Washington, D.C.: AGU; 1984. p. 158-168. https://doi.org/10.1029/GM028p0158
32. Madelaire M, Laundal KM, Reistad JP, Hatch SM, Ohma A, Haaland S. Geomagnetic response to rapid increases in solar wind dynamic pressure: Event detection and large scale response. Front Astron Space Sci. 2022;9:904620. https://doi.org/10.3389/fspas.2022.904620
33. Mayaud PN, editor. Derivation, meaning, and use of geomagnetic indices. Geophys Monogr Ser. Vol. 22. Washington, D.C.: AGU; 1980. https://doi.org/10.1029/GM022
34. McPherron RL. Substorm-related changes in the geomagnetic tail: The growth phase. Planet Space Sci. 1972;20:1521-1539. https://doi.org/10.1016/0032-0633(72)90054-2
35. Nakai H, Kamide Y. Response of nightside auroral-oval boundaries to the interplanetary magnetic field. J Geophys Res Space Phys. 1983;88:4005-4014. https://doi.org/10.1029/JA088iA05p04005
36. Newell P, Gjerloev J. Substorm and magnetosphere characteristic scales inferred from the SuperMAG auroral electrojet indices. J Geophys Res Space Phys. 2011;116:A12211. https://doi.org/10.1029/2011JA016936
37. Newell PT, Sotirelis T, Liou K, Rich FJ. Pairs of solar wind-magnetosphere coupling functions: Combining a merging term with a viscous term works best. J Geophys Res Space Phys. 2008;113:A04218. https://doi.org/10.1029/2007JA012825
38. Nishimura Y, Bruus E, Karvinen E, Martinis CR, Dyer A, Kangas L, *et al*. Interaction between proton aurora and stable auroral red arcs unveiled by citizen scientist photographs. J Geophys Res Space Phys. 2022;127:e2022JA030570. https://doi.org/10.1029/2022JA030570
39. O'Brien TP. SEAES-GEO: A spacecraft environmental anomalies expert system for geosynchronous orbit. Space Weather. 2009;7:S09003. https://doi.org/10.1029/2009SW000473
40. Rich FJ, Hairston MR. Large-scale convection patterns observed by DMSO. J Geophys Res. 1994;99(A3):3827-3844. https://doi.org/10.1029/93JA03296
41. Richardson IG, Cane HV. Solar wind driver of geomagnetic storms during more than four solar cycles. J Space Weather Space Clim. 2012;2:A01. https://doi.org/10.1051/swsc/2012001
42. Reiff PH, Spiro RW, Hill TW. Dependence of polar cap potential drop on interplanetary parameters. J Geophys Res. 1981;86:7639-7648. https://doi.org/10.1029/JA086iA09p07639
43. Rostoker G, Akasofu SI, Foster J, Greenwald RA, Kamide Y, Kawasaki K, *et al*. Magnetospheric substorms—definition and signatures. J Geophys Res Space Phys. 1980;85:1663-1668. https://doi.org/10.1029/JA085iA04p01663
44. Russell H, Elphic RC. ISEE observations of flux transfer events at the dayside magnetopause. Geophys Res Lett. 1979;6(1):33-36. https://doi.org/10.1029/GL006i001p00033
45. Shi Y, Moldwin MB. Interhemispheric asymmetries in magnetosphere and ionosphere magnetic field residuals between Swarm observations and Earth magnetic field models. J Geophys Res Space Phys. 2022;127:e2021JA030190. https://doi.org/10.1029/2021JA030190
46. Shue JH, Newell PT, Liou K, Meng CI. Solar wind density and velocity control of auroral brightness under normal interplanetary magnetic field conditions. J Geophys Res. 2002;107(A10):1296. https://doi.org/10.1029/2001JA009138
47. Shue JH, Newell PT, Liou K, Meng CI. The quantitative relationship between auroral brightness and solar EUV Pedersen conductance. J Geophys Res. 2001;106:5883-5892. https://doi.org/10.1029/2000JA003002
48. Snyder CW, Neugebauer M, Rao UR. The solar wind velocity and its correlation with cosmic-ray variations and with solar and geomagnetic activity. J Geophys Res. 1963;68(24):6361-6370. https://doi.org/10.1029/JZ068i024p06361
49. Thomsen MF. Why KP is such a good measure of magnetospheric convection. Space Weather. 2004;2:S11004. https://doi.org/10.1029/2004SW000089
50. Vichare G, Bhaskar A, Rawat R, Yadav V, Mishra W, Angchuk D, Singh AK. Low-latitude auroras: Insights from 23 April 2023 solar storm. arXiv. 2024. https://doi.org/10.48550/arXiv.2405.08821
51. Wing S, Newell PT, Sibeck DG, Baker KB. A large statistical study of the entry of interplanetary magnetic field Y-component into the magnetosphere. Geophys Res Lett. 1995;22:2083-2086. https://doi.org/10.1029/95GL02261